Direct demonstration of discrete Ca^{2+} microdomains associated with different isoforms of adenylyl cyclase

Debbie Willoughby, Sebastian Wachten, Nanako Masada and Dermot M. F. Cooper*

Department of Pharmacology, Tennis Court Road, University of Cambridge, CB2 1PD, UK

*Author for correspondence (dmfc2@cam.ac.uk)

Accepted 3 November 2009
Journal of Cell Science 123, 107-117 Published by The Company of Biologists 2010
doi:10.1242/jcs.062067

Summary

Ca^{2+}-sensitive adenylyl cyclases (ACs) orchestrate dynamic interplay between Ca^{2+} and cAMP that is a crucial feature of cellular homeostasis. Significantly, these ACs are highly selective for capacitative Ca^{2+} entry (CCE) over other modes of Ca^{2+} increase. To directly address the possibility that these ACs reside in discrete Ca^{2+} microdomains, we tethered a Ca^{2+} sensor, GCaMP2, to the N-terminus of Ca^{2+}-stimulated AC8. GCaMP2-AC8 measurements were compared with global, plasma membrane (PM)-targeted or Ca^{2+}-insensitive AC2-targeted GCaMP2. In intact cells, GCaMP2-AC8 responded rapidly to CCE, but was largely unresponsive to other types of Ca^{2+} rise. The global GCaMP2, PM-targeted GCaMP2 and GCaMP2-AC2 sensors reported large Ca^{2+} fluxes during Ca^{2+} mobilization and non-specific Ca^{2+} entry, but were less responsive to CCE than GCaMP2-AC8. Our data reveal that different AC isoforms localize to distinct Ca^{2+}-microdomains within the plasma membrane. AC2, which is regulated via protein kinase C, resides in a microdomain that is exposed to a range of widespread Ca^{2+} signals seen throughout the cytosol. By contrast, a unique Ca^{2+} microdomain surrounds AC8 that promotes selectivity for Ca^{2+} signals arising from CCE, and optimizes CCE-mediated cAMP synthesis. This direct demonstration of discrete compartmentalized Ca^{2+} signals associated with specific signalling proteins provides a remarkable insight into the functional organization of signalling microdomains.

Key words: cAMP, GCaMP2, Compartmentalization

Introduction

Direct interplay between Ca^{2+} and cAMP signalling is fundamental to some of the most elaborate aspects of cellular homeostasis, including hormone and neurotransmitter release, cardiac contraction, cell migration and synaptic development (Abrams et al., 1991; Ferguson and Storm, 2004; Nicol et al., 2006; Rapp and Berridge, 1977; Rasmussen and Goodman, 1977). To a considerable extent, the co-ordinated interaction between these two ubiquitous messengers is controlled by the Ca^{2+}-sensitive adenylyl cyclases (AC1, AC5, AC6 and AC8) (Cooper et al., 1995). AC1 and AC8 are stimulated by Ca^{2+} in a calmodulin (CaM)-dependent manner (Cali et al., 1994; Wu et al., 1993), whereas AC5 and AC6 are directly inhibited by Ca^{2+} (Guillou et al., 1999; Yoshimura and Cooper, 1992). Recent evidence suggests that the exquisite sensitivity of these ACs for Ca^{2+} in the submicromolar range, coupled with distinct subcellular localization of Ca^{2+}-sensitive AC isoforms (Willoughby and Cooper, 2007), can give rise to temporally and spatially distinct patterns of cAMP signal in response to dynamic intracellular Ca^{2+} events (Dyachok et al., 2006; Landa et al., 2005; Willoughby and Cooper, 2006).

Previous studies have demonstrated a robust selectivity of the Ca^{2+}-sensitive ACs for distinct modes of Ca^{2+} increase. In particular, the ACs are uniquely sensitive to Ca^{2+} rises mediated by capacitative Ca^{2+} entry (CCE), which occurs as a consequence of endoplasmic reticulum (ER) store depletion. This depletion follows either inositol-(1,4,5)-trisphosphate [Ins(1,4,5)P_3]-mediated Ca^{2+} release or pharmacologically induced passive store depletion using sarcoplasmic/endoplasmic reticulum calcium ATPase (SERCA) pump inhibitors, such as thapsigargin (Tg) (Chiono et al., 1995; Fagan et al., 1996; Fagan et al., 1998). Surprisingly, even in excitable cells, a relatively modest CCE can influence AC activity to a similar degree as that produced by much larger Ca^{2+} signals arising from voltage-gated Ca^{2+} channel activity (Fagan et al., 2000a). By contrast, the Ca^{2+}-sensitive ACs display remarkably limited sensitivity to Ins(1,4,5)P_3-mediated Ca^{2+} release from the ER in the absence of external Ca^{2+} and to other forms of Ca^{2+} entry mediated by ionophore, arachidonic acid or 1-oleoyl-2-acetyl-sn-glycerol (OAG) (Fagan et al., 1996; Martin and Cooper, 2006; Shuttleworth and Thompson, 1999). Thus, despite the enzymes displaying a simple dose-dependent Ca^{2+} sensitivity in vitro, in the intact cell, equivalent (or higher) Ca^{2+} rises originating from non-CCE sources are far less effective at regulating the ACs. The reason for this selectivity is currently unknown. Functional studies have indirectly suggested that a close association between AC8 and CCE channels might underlie the phenomenon (Gu and Cooper, 2000; Martin et al., 2009). This is supported by the targeting of Ca^{2+}-sensitive ACs and key CCE proteins to sphingolipid and cholesterol-rich regions of the plasma membrane (PM), known as lipid rafts (a subset of which are the morphologically identifiable caveolae) (Fagan et al., 2000b; Smith et al., 2002). A flourish of interest in the recently identified molecular components of CCE, stromal interaction molecule 1 (STIM1) and Orai1, has revealed that these proteins, along with the type 1 canonical transient receptor potential channel (TRPC1), locate to lipid rafts during store depletion (Alicia et al., 2008; Pani et al., 2008). Further evidence that CCE signals originate in these domains has been provided using a genetically encoded GFP-based Ca^{2+} 'cameleon' sensor attached to the lipid-raft marker caveolin-1, to directly monitor Ca^{2+} in these PM microdomains during CCE (Isshiki et al., 2002).

Despite circumstantial evidence that sub-plasmalemmal and global Ca^{2+} signals can differ greatly (Marsault et al., 1997), a direct observation of a discrete Ca^{2+} pool within the sub-plasmalemmal AC8 microenvironment has not been made. Furthermore, there are no data to indicate how Ca^{2+} signals within the microdomains of

raft-targeted Ca^{2+}-sensitive ACs might differ from those occurring near other non-raft-targeted particulate ACs. In the present study, we have tethered the genetically encoded, high-affinity Ca^{2+} sensor, GCaMP2 (Tallini et al., 2006), to the N-terminus of the raft-localized Ca^{2+}-sensitive AC, AC8. This approach has enabled the first direct monitoring of Ca^{2+} changes within the immediate vicinity of AC8. Comparisons were made between this sensor (GCaMP2-AC8) and GCaMP2 when attached to the N-terminus of AC2 (a Ca^{2+}-insensitive, non-raft-targeted AC; GCaMP2-AC2) when expressed in the cytosol (global GCaMP2) or when targeted to the PM (PM-GCaMP2) in HEK293 cells. Our results provide definitive evidence that AC8 resides in a discrete 'microdomain' of the cell that is exposed to rapid fluctuations in Ca^{2+} during CCE. Furthermore, AC8 is uniquely shielded from other modes of Ca^{2+} increase, such as ionomycin-mediated Ca^{2+} entry, which generates large, global Ca^{2+} signals. By contrast, the non-raft-targeted AC2 is exposed to significant Ca^{2+} rises during Ca^{2+} mobilization from ER stores and non-specific Ca^{2+}-entry; however, exposure of AC2 to store-operated Ca^{2+} entry is clearly delayed. The remarkably different Ca^{2+} signals seen within the vicinity of AC8 and AC2 suggest that these ACs localize to architecturally distinct sub-plasmalemmal regions and might underpin the diverse regulatory actions of these ACs within the cell.

Results

Design and characterization of AC-tethered GCaMP2 constructs

GCaMP2 is a genetically encoded, high-affinity Ca^{2+} sensor that exhibits large fluorescent shifts in response to physiological Ca^{2+} changes (Lee et al., 2006; Tallini et al., 2006). The sensor comprises a circularly permuted EGFP flanked by CaM and a CaM-binding peptide (M13) from myosin light chain kinase. Increases in Ca^{2+} promote Ca^{2+}-CaM-M13 interaction and a conformational change within the sensor, resulting in an increase in EGFP fluorescence (Nakai et al., 2001; Tallini et al., 2006). Recently, GCaMP2 has also been attached to specific proteins so that it can be targeted to explicit sites within the cell, including junctional sites between the ER and PM ('plasmerosomes') and dendritic spines to examine Ca^{2+} signals within these cellular microdomains (Lee et al., 2006; Mao et al., 2008).

We have developed a number of targeted GCaMP2 constructs in order to monitor Ca^{2+} changes in specific subcellular regions. For

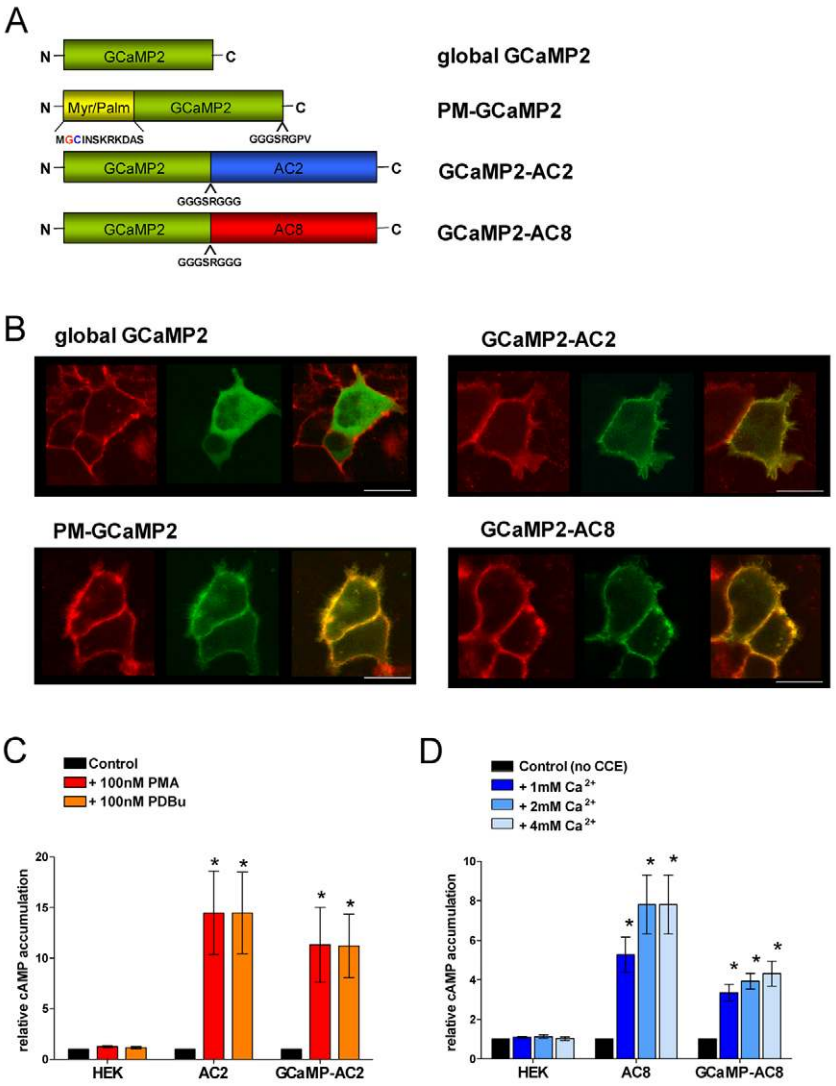

Fig. 1. Design and characterization of AC-targeted GCaMP2 constructs. (**A**) Schematic representation of the four GCaMP2-based constructs used in this study. An N-terminal modification containing the 'SH4' motif (GCINSKRKD) of Lyn kinase was introduced to generate a myristoylated and palmitoylated (Myr/Palm) version of GCaMP2, termed PM-GCaMP2. GCaMP2 was also linked to the N-terminus of full-length sequence for AC2 or AC8 via the amino acid linker GGGSRGGG. (**B**) Localization of the GCaMP2 sensors when transiently expressed in HEK293 cells. All confocal images were obtained at 40× magnification during excitation at 633 nm to excite the CellMask Deep Red plasma membrane stain (red) or 488 nm light to excite GCaMP2 constructs (green). Overlays of images from both channels are also presented to identify regions of signal colocalization (yellow). Scale bars: 20 µm. (**C**) Cell population cAMP accumulation data examining the effects of phorbol myristate acetate (PMA, 100 nM) or phorbol dibutyrate (PDBu, 100 nM) on wild-type versus GCaMP2-tagged AC2 activity in a 15-minute cAMP accumulation assay in the presence of 100 nM FSK and 100 µM IBMX. (**D**) Comparison of the CCE sensitivity of GCaMP2-AC8 compared with wild-type AC8 and untransfected HEK293 cells. Cells were pretreated with 100 nM Tg and the cAMP accumulation in the presence of 1 µM FSK and 100 µM IBMX was measured over the 1-minute period following addition of external Ca^{2+} (1, 2 or 4 mM) to trigger CCE. Data are presented as mean values ± s.d. (n=3), *P<0.05 (Student's t-test).

near-membrane Ca^{2+} measurements, a plasma-membrane-targeted version of GCaMP2 was generated by the addition of an 'SH4' sequence motif derived from Lyn kinase. This sequence is modified to generate a palmitoylation and myristoylation group at the N-terminus of GCaMP2, which effectively targets the sensor to the PM (this new construct is referred to as PM-GCaMP2, see Fig. 1A). For more localized Ca^{2+} measurements within the immediate vicinity of specific AC isoforms, GCaMP2 was attached to the N-terminus of full-length AC2 and AC8 to generate GCaMP2-AC2 and GCaMP2-AC8, respectively (Fig. 1A). Ca^{2+}-stimulated AC8 is thought to reside in lipid rafts (Fagan et al., 2000b; Smith et al., 2002), and Ca^{2+}-insensitive AC2 to reside in non-raft regions of the plasma membrane (Cooper and Crossthwaite, 2006). To examine the distribution of the sensors when transiently expressed in HEK293 cells, live-cell confocal imaging was used to compare expression patterns of each of the four GCaMP2-based sensors with a PM stain (CellMask Deep Red). Fig. 1B demonstrates good colocalization of PM-GCaMP2, GCaMP2-AC2 and GCaMP2-AC8 with the CellMask PM marker. PM-GCaMP2 and GCaMP2-AC8 consistently displayed good colocalization with the PM marker, but expression of GCaMP2-AC2 was more variable from cell to cell and was retained within the Golgi in some cells (a similar distribution pattern is seen with HA-tagged AC2; our unpublished results). Consequently, only cells clearly expressing GCaMP2-AC2 at the PM were selected for single-cell Ca^{2+} measurements. By contrast, untagged GCaMP2 was expressed within the cytosol and did not colocalize with the PM marker.

To determine whether fusion with GCaMP2 impaired the responsiveness of the ACs to physiological stimuli cell population, cAMP assays were conducted in HEK293 cells expressing either wild-type or GCaMP2-tagged versions of AC2 and AC8. Previous studies have shown that Ca^{2+}-insensitive AC2 can be readily stimulated by protein kinase C (PKC) (Jacobowitz et al., 1993; Yoshimura and Cooper, 1993). Cell population cAMP assay data presented in Fig. 1C revealed significant enhancement of GCaMP2-tagged AC2 activity during treatment with the phorbol esters, phorbol myristate acetate (PMA, 100 nM) or phorbol dibutyrate (PDBu, 100 nM). Accumulation of cAMP levels in GCaMP2-AC2-expressing cells over a 15-minute period was comparable to that seen in cells expressing wild-type AC2, which confirmed that the tagged AC2 was localized to the same regulatory domains of the PM as the wild-type homologue. A comparison of GCaMP2-AC8 and wild-type AC8 activity during a 1-minute period of CCE, following prior store depletion using 100 nM Tg in Ca^{2+}-free conditions, revealed that both versions of AC8 responded well to increasing degrees of CCE (Fig. 1D). These data confirmed that GCaMP2-AC8 was correctly targeted to regions of the PM associated with CCE. Furthermore, CaM present within the GCaMP2 itself did not directly affect the Ca^{2+} regulation of GCaMP2-AC8, which is dependent on the pre-association of endogenous CaM at the N-terminus of AC8 (Simpson et al., 2006; McDougall et al., 2009). Thus, we concluded that attachment of the GFP-based Ca^{2+} sensor did not disrupt the functionality of AC8 or its sensitivity to CCE.

In situ calibrations for the GCaMP2-based sensors were performed to confirm that the sensitivity of GCaMP2 to Ca^{2+} was not compromised when PM-targeting motifs, or specific AC isoforms, were tethered to the N- or C-termini, respectively (supplementary material Fig. S1A). The in situ calibrations revealed that all four GCaMP2-based sensors displayed submicromolar sensitivity to Ca^{2+}, with the dissociation constant (K_d) values estimated at 171 nM for global GCaMP2, 234 nM for PM-GCaMP2, 240 nM for GCaMP2-AC2 and 311 nM for GCaMP2-AC8. The K_d value for the global sensor was comparable to that reported by others (Lee et al., 2006; Tallini et al., 2006). Modifications to GCaMP2 generated small decreases in the Ca^{2+} sensitivity of the probe but did not limit the use of the new sensors over the physiological Ca^{2+} range (up to ~800 nM). In agreement with previous reports, Hill coefficients for all four GCaMP2-based sensors were estimated to be ~3 (Lee et al., 2006; Tallini et al., 2006).

Selective responsiveness of AC8 to CCE at the single-cell level

Previous studies in cell populations have demonstrated robust, dose-dependent, stimulation of AC8 by CCE when expressed in HEK293 cells (Fagan et al., 1998). By contrast, Ins(1,4,5)P_3-mediated Ca^{2+} mobilization from the ER, in the absence of external Ca^{2+}, is only a modest stimulator of AC8 activity in cell populations (Fagan et al., 1998). Prior to examining the subcellular [Ca^{2+}] changes detected by our newly designed GCaMP2-based sensors, we first analysed the effects of Ins(1,4,5)P_3-induced Ca^{2+} release and CCE on cAMP production in individual HEK293 cells stably expressing AC8 (HEK-AC8) (Fig. 2). To monitor changes in cAMP production, the cytosolic FRET-based cAMP sensor Epac2-camps (Nikolaev et al., 2004) was transiently expressed in the HEK-AC8 cells. Addition of a muscarinic agonist, carbachol (CCh; 500 μM), in Ca^{2+}-free conditions mobilized ER stores to generate a large rise in cytosolic [Ca^{2+}], as detected with the ratiometric Ca^{2+} indicator Fura-2 (Fig. 2A). In parallel real-time cAMP measurements, the majority of cells (39 out of 67 cells tested) exhibited no increase in cAMP production during Ca^{2+} mobilization from the ER (see Fig. 2B, top panel for example traces). The remaining 28 cells displayed varying degrees of cAMP production in response to the Ins(1,4,5)P_3-mediated Ca^{2+} signal (see Fig. 2B, bottom panel for example traces from three individual cells). Such variability of cAMP production in response to ER Ca^{2+} release at the single-cell level is perhaps consistent with the modest stimulation of AC8 activity seen in cell population assays (Fagan et al., 1998). The subsequent addition of 2 mM external Ca^{2+} to trigger CCE (Fig. 2A, top panel) was accompanied by enhanced cAMP production in all cells tested (Fig. 2B). Data analyses revealed that, on average, CCE produced a twofold greater increase in cAMP production in HEK-AC8 cells than CCh-induced Ca^{2+} mobilization (Fig. 2C). Prior ER store depletion using either the SERCA pump inhibitor Tg (100 nM) or the Ca^{2+} ionophore ionomycin (IM; 200 nM) abolished the effects of CCh on cAMP production in Ca^{2}-free conditions. This confirmed that the stimulatory actions of CCh on cAMP production observed in ~40% of cells in Ca^{2+}-free conditions were mediated by Ca^{2+} mobilization from ER stores. Subsequent CCE induced by the addition of 2 mM Ca^{2+} to the bath solution, following Tg- or IM-induced ER store depletion, produced significant AC8 activity (Fig. 2C; n=65 or 20 cells, respectively). The scatter plot in Fig. 2D compares peak cAMP production in response to Ca^{2+} release from the ER with CCE in individual HEK-AC8 cells and demonstrates a bias towards stimulation of AC8 by CCE. These data are consistent with the hypothesis that a close association between AC8 and sites of CCE renders the AC selective for CCE over Ca^{2+} release from intracellular stores. However, it should be noted that a significant subpopulation of HEK-AC8 cells were found to be equally responsive to both release and entry. Fura-2 measurements in HEK-AC8 cells revealed that CCh addition in Ca^{2+}-free conditions resulted in a marked Ca^{2+} rise in all cells tested (Fig. 2A),

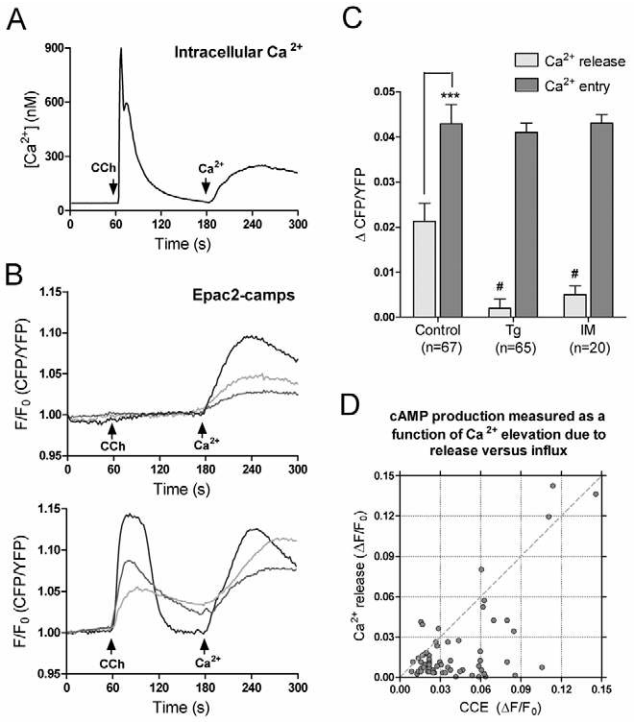

Fig. 2. Stimulation of AC8 by CCh-induced Ca^{2+} release versus CCE at the single-cell level. (**A**) Intracellular Ca^{2+} changes evoked by 500 μM CCh-induced Ca^{2+} release and subsequent CCE (addition of 2 mM external Ca^{2+}) in Fura-2-loaded cells (average response from 100 cells). (**B**) Changes in cAMP levels in single HEK-AC8 cells monitored using Epac2-camps. Three example traces are shown for cells that did not respond to Ca^{2+} mobilization (top) and cells that did (bottom). (**C**) Average effects of CCh-induced Ca^{2+} release and subsequent CCE under control conditions and following prior store depletion with either 100nM Tg or 200 nM IM. Data are plotted as mean ± s.e.m. ***P<0.001 for comparison of release and entry under control conditions; $^{\#}P$<0.001 when comparing the effects of Ca^{2+} release following Tg or IM pretreatment to the effects of release under control conditions. (**D**) Scatter plot analysis of the peak change in Epac2-camps FRET ratio during CCh-induced Ca^{2+} mobilization and subsequent CCE in all HEK-AC8 cells tested (n=67).

suggesting that such variable cAMP responses (Fig. 2B) might reflect differential targeting and/or expression levels of AC8 in the two different subpopulations.

Ca^{2+} shifts in the immediate vicinities of AC2 and AC8

GCaMP2-AC8 and GCaMP2-AC2 constructs were expressed in HEK293 cells in order to monitor Ca^{2+} signals in the subcellular regions directly adjacent to the two AC isoforms. This experimental approach enabled us to unequivocally address whether AC8 resides in a unique microdomain of the cell that is exposed to greater Ca^{2+} shifts as a consequence of CCE than during ER store release. Using the same protocol to induce Ca^{2+} mobilization and CCE as described above, we examined local changes in Ca^{2+} in the immediate vicinities of AC8 and the Ca^{2+}-insensitive AC2. Changes in Ca^{2+} were also assessed using global or PM-targeted GCaMP2 sensors. Representative traces of fluorescent intensity shifts for each GCaMP2 construct are presented in Fig. 3A-D alongside scatter plot analyses of the peak responses of each sensor to Ca^{2+} release and entry in all cells tested (n values range from 34 to 89).

Our findings illustrate large transient Ca^{2+} increases with the global, PM-targeted and AC2-tagged GCaMP2 sensors during CCh-evoked Ca^{2+} release from the ER. Subsequent addition of 2 mM external Ca^{2+} was accompanied by the detection of further increases in [Ca^{2+}] (Fig. 3A-C). Despite targeting of GCaMP2-AC2 to microdomains within the PM, the dynamics of the local Ca^{2+} signals were similar to those detected with the global GCaMP2 sensor, displaying a gradual signal increase during Ca^{2+} entry. This response is comparable to the cytosolic Ca^{2+} changes measured using Fura-2 under the same experimental conditions (Fig. 2A). By contrast, PM-GCaMP2 detected a dampening oscillatory response to Ins(1,4,5)P_3-mediated Ca^{2+} release, suggesting that some of the mobilizable Ca^{2+} originated from, and was rapidly sequestered by, ER in close proximity to the PM. Notably, the initial response of PM-GCaMP2 to CCE (Fig. 3B) was larger and significantly faster than that detected by the global or the AC2-targeted sensor (Fig. 3A,C), consistent with a closer localization of PM-GCaMP2 to sites of Ca^{2+} entry. Data analyses show that the peak response of all three GCaMP2 sensors to Ca^{2+} mobilization was consistently larger (in >90% of cells tested) than that induced by CCE (Fig. 3A-C, scatter plots). By striking contrast, 67% of GCaMP2-AC8-expressing cells (60 out of 89 cells tested) detected little or no change in local Ca^{2+} levels during CCh-evoked Ca^{2+} release (e.g. Fig. 3D, cell 1), indicating that AC8 might reside at sites within the PM that are 'distant' or 'shielded' from Ins(1,4,5)P_3-receptor-mediated Ca^{2+} signals. The remaining GCaMP2-AC8 cells reported a modest transient rise in fluorescent signal during CCh-evoked Ca^{2+} release (Fig. 3D, cell 2). Typically, those cells expressing GCaMP2-AC8 that did not respond to Ca^{2+} release produced rapid and significant fluorescent shifts on induction of CCE (e.g. Fig. 3D, cell 1). Cells in which GCaMP2-AC8 detected a moderate response to release exhibited a weaker signal for CCE (e.g. Fig. 3D, cell 2) with dynamics comparable to global GCaMP2 measurements. Our observation of two subpopulations of GCaMP2-AC8-expressing HEK293 cells (either responsive or non-responsive to Ca^{2+} release) was consistent with the variable cAMP responses seen during Ca^{2+} mobilization (Fig. 2B). Scatter plot analysis of GCaMP2-AC8-expressing cells (Fig. 3D, right hand panel) revealed that this Ca^{2+} sensor preferentially detected CCE events rather than Ca^{2+} release. Furthermore, GCaMP2-AC8 was far more responsive to CCE than any of the other GCaMP2 probes.

These findings are reflected in Fig. 3E, which presents data for the peak GCaMP2 signal increase in response to Ca^{2+} release relative to CCE for each construct. The ability of the global GCaMP2 sensor to detect much larger fluxes during Ca^{2+} release compared with CCE was significantly reduced in cells expressing GCaMP2-AC8 [4.76±0.74 for global GCaMP2 (n=75 cells) compared with just 0.94±0.13 for GCaMP2-AC8 (n=89 cells); P<0.001]. Interestingly, the non-raft-localized GCaMP2-AC2 was even more responsive to release than entry (7.26±0.91, n=34) compared with global GCaMP2 measurements (*P<0.05). Both PM-GCaMP2 and GCaMP2-AC8 exhibited significantly faster responses to CCE (30.2±2.3 and 24.4±2.0 seconds to peak, respectively) compared with global or AC2-tagged GCaMP2 (89.0±4.3 and 77.4±5.2 seconds to peak, respectively). Further analyses from cells expressing PM-GCaMP2 and GCaMP2-AC8 revealed that in 88% and 95% of cells, respectively, the sensors detected a peak Ca^{2+} increase during the first minute of CCE, with the peak response detected within the first 30 seconds in the majority of cells (Fig. 3G,I). Our data suggest that these two sensors localize relatively close to sites of CCE. By contrast, in just 25% of cells expressing global GCaMP2 or GCaMP2-AC2 the sensors detected a peak rise in Ca^{2+} entry within the first minute of CCE (Fig. 3F,H).

AC8 resides close to sites of CCE

The selectivity of AC8 for Ca^{2+} entering via CCE channels is hypothesized to be a consequence of intimacy between the Ca^{2+} stimulatable enzyme and the molecular components of CCE channels. This is supported by recent work from our laboratory, which revealed that overexpression of STIM1 and Orai in HEK293 cells produced a marked increase in CCE that was accompanied by a proportional enhancement of AC8 activity. By contrast,

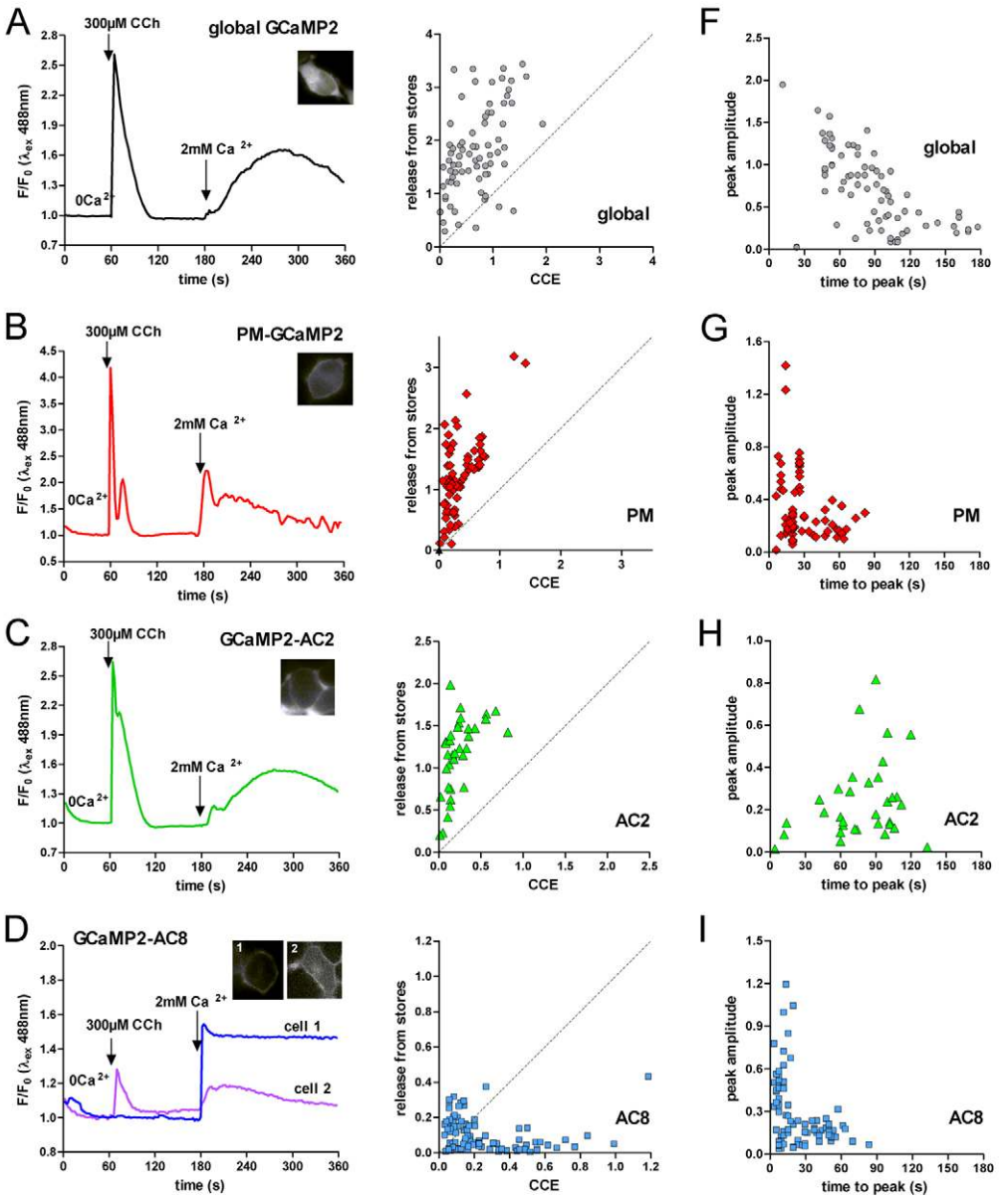

E

	Ca^{2+} release : CCE	Time to CCE peak (s)	n value
global GCaMP2	4.76 ± 0.74	89.0 ± 4.3	75
PM-GCaMP2	5.07 ± 0.47	30.2 ± 2.3***	69
GCaMP2-AC2	7.26 ± 0.91 *	77.4 ± 5.2	34
GCaMP2-AC8	0.94 ± 0.13 ***	24.4 ± 2.0***	89

Fig. 3. Selectivity of GCaMP2-AC8 for detection of Ca^{2+} changes associated with CCE rather than Ins(1,4,5)P_3-mediated Ca^{2+} release from the ER. (**A**) Left hand panel: example trace of Ca^{2+} changes detected with the global GCaMP2 sensor during 300 μM CCh-induced Ca^{2+} release and subsequent CCE induced by the addition of 2 mM Ca^{2+}. Right hand panel: scatter plot of the peak response of the global GCaMP2 sensor to Ca^{2+} mobilization versus CCE in all cells tested (n=75). (**B-D**), Example traces from individual cells and scatter plots comparing the effects of peak release versus peak entry on local Ca^{2+} signals detected with PM-GCaMP2 (n=69), GCaMP2-AC2 (n=34) and GCaMP2-AC8 (n=89). (**E**) Relative sensitivity of each sensor for Ca^{2+} release compared with CCE and the time taken to reach peak signal increase following the induction of CCE (*P<0.05, ***P<0.001 compared with global). (**F-I**), Scatter plots for global, PM-, AC2- and AC8-tagged versions of GCaMP2 showing time to reach peak signal increase as a consequence of CCE.

pharmacological disruption of STIM1 recruitment to lipid-raft regions of the PM significantly reduced CCE-dependent AC8 activity (Martin et al., 2009).

Here, we loaded HEK293 cells with Ca^{2+} chelators (EGTA and BAPTA) to examine the adjacency of the GCaMP2-based sensors to sites of Ca^{2+} entry during CCh-evoked CCE. EGTA and BAPTA have similar binding affinities for Ca^{2+}; however, the on-rate of BAPTA for Ca^{2+} is ~150 times faster than that for EGTA (Naraghi and Neher, 1997). Consequently, EGTA is less effective at limiting the diffusion of Ca^{2+} away from its site of entry than an equivalent BAPTA concentration and might not be expected to impede the detection of Ca^{2+} by GCaMP2 sensors that reside very close to sites of CCE. Loading conditions for the acetoxymethyl esters of BAPTA and EGTA were established using Fura-2 to test the effectiveness of a range of EGTA-AM and BAPTA-AM concentrations at chelating Ca^{2+} that entered the cell during CCE (see supplementary material Fig. S2). Loading for 45 minutes with 30 μM EGTA-AM or 30 μM BAPTA-AM was found to be equally effective at minimizing Ca^{2+} entry, as measured using Fura-2. Consistent with the hypothesis that AC8 resides close to sites of CCE, pre-incubation with 30 μM EGTA-AM did not significantly attenuate the initial detection of Ca^{2+} entry in HEK293 cells expressing GCaMP2-AC8 (Fig. 4D). Although the plateau phase for CCE detected with GCaMP2-AC8 in the presence of EGTA was reduced, the early response was equivalent to 92±3% of that seen under control conditions. The CCE-mediated Ca^{2+} signal detected by GCaMP2-AC8 was completely ablated following loading of the fast Ca^{2+} chelator BAPTA (Fig. 4D). Although PM-GCaMP2 could detect relatively rapid increases in sub-plasmalemmal Ca^{2+} following stimulation of CCE (Fig. 3G), loading with EGTA-AM prevented the detection of CCE-evoked Ca^{2+} signals by this sensor (Fig. 4B). The data suggest that PM-GCaMP2 is targeted to sites that are more distant from CCE channels than is GCaMP2-AC8. Both the global GCaMP2 (Fig. 4A) and GCaMP2-AC2 (Fig. 4C) probes did not detect any obvious Ca^{2+} shifts following loading with either EGTA or BAPTA. The inability of these sensors to discriminate between the two Ca^{2+} chelators implies that they do not reside close to the source of the Ca^{2+} rise, and that although AC8 associates very closely with sites of CCE, AC2 must locate to a region of the PM that is relatively distant from CCE channels.

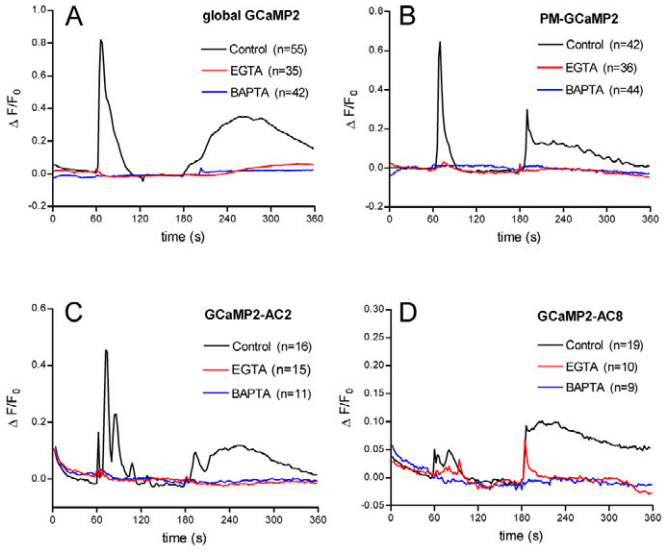

Fig. 4. Effects of EGTA and BAPTA on local Ca^{2+} signals. (**A**) Average traces of Ca^{2+} signals detected with global GCaMP2 following 45-minute pre-incubation of cells with either 30 μM EGTA-AM or 30 μM BAPTA-AM. Similar data are plotted for (**B**) PM-GCaMP2, (**C**) GCaMP2-AC2 and (**D**) GCaMP2-AC8.

Comparison of the effects of non-specific Ca^{2+} entry on GCaMP2 constructs

A striking characteristic of AC8 is its insensitivity to non-specific Ca^{2+} entry mediated by the Ca^{2+} ionophore IM (Fagan et al., 1996). Treatment of HEK293-AC8 cells with 4 μM IM in Ca^{2+}-free conditions resulted in a large transient rise in cytosolic Ca^{2+} levels (as measured with Fura-2) as Ca^{2+} is released from intracellular organelles including the ER and mitochondria (Fig. 5A). After subsequent addition of 0.5 mM extracellular Ca^{2+}, a large sustained rise in cytosolic Ca^{2+} was seen (Fig. 5A). A small component of

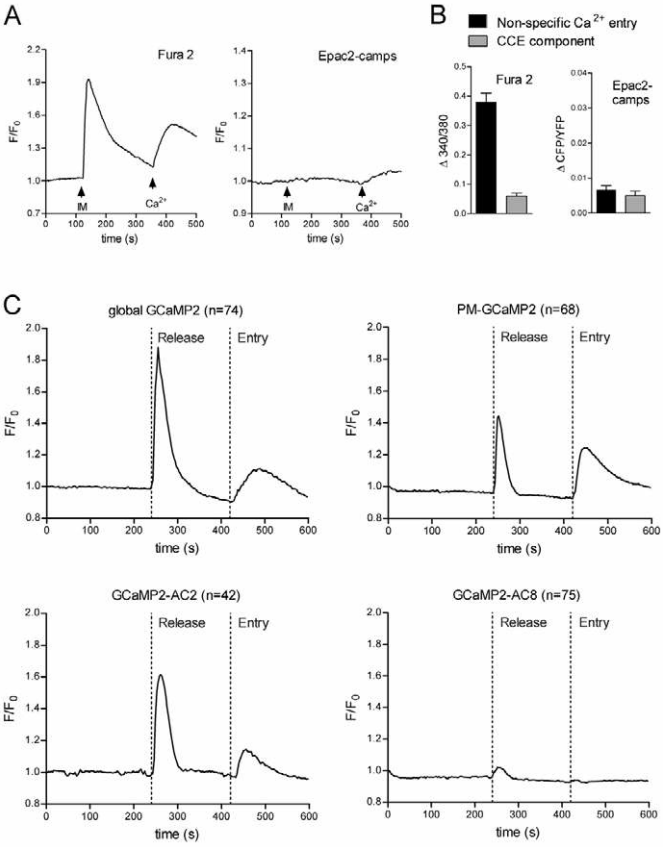

Fig. 5. GCaMP2-AC8 resides in a subdomain of the plasma membrane that is shielded from ionophore-mediated Ca^{2+} signals. (**A**) Fura-2 and Epac2-camps measurements of ionophore-mediated effects on Ca^{2+} and cAMP changes, respectively. IM (4 μM) was added at 120 seconds in Ca^{2+}-free conditions to empty internal Ca^{2+} stores. Subsequent addition of 0.5 mM external Ca^{2+} at 360 seconds triggered a combination of non-specific Ca^{2+} entry and CCE. (**B**) Average data showing the relative contributions of either non-specific Ca^{2+} entry or CCE to Ca^{2+} and cAMP changes. (**C**) Responses of the four GCaMP2-based sensors to non-specific Ca^{2+} entry, corrected for any contributions from CCE. Cells were pretreated with 200 nM Tg, and 4 μM IM was added at 270 seconds. External Ca^{2+} (0.5 mM) was introduced at 420 seconds.

the latter signal is mediated by CCE (as a result of ER stores emptying) whereas the bulk of the rise is due to non-specific Ca^{2+} entry (Fig. 5B). The CCE component of the response was estimated from Fura-2 measurements in which cells were pretreated with Tg (200 nM) rather than IM prior to the addition of 0.5 mM external Ca^{2+}. Parallel experiments using the cytosolic FRET-based cAMP sensor Epac2-camps revealed that non-specific Ca^{2+} entry, induced by IM treatment, did not significantly influence cAMP production in HEK293-AC8 cells (Fig. 5A, right hand panel). Only a small increase in cAMP was seen on addition of 0.5 mM external Ca^{2+}; this was attributable to CCE rather than to non-specific Ca^{2+} entry, as confirmed by parallel experiments that measured the effects of Tg-induced CCE (0.5 mM external Ca^{2+}) in the absence of IM (Fig. 5B). This apparent insensitivity of AC8 to large fluxes in Ca^{2+} as a consequence of ionophore-mediated Ca^{2+} entry points to either a direct link between CCE and AC8 activity (potentially mediated via direct protein-protein interactions), or to the residence of AC8 in a subcellular microdomain that is 'shielded' from ionophore-mediated Ca^{2+} rises.

To address the latter point, the four GCaMP2-based sensors were used to directly monitor local Ca^{2+} changes within the different cellular domains during IM treatment (Fig. 5C). All cells were pretreated with Tg (200 nM) to deplete ER Ca^{2+} stores. Parallel experiments were then performed with and without IM (4 μM) to estimate the Ca^{2+} shifts seen as a consequence of non-specific Ca^{2+} entry as well as the small CCE component detected by each sensor after the addition of 0.5 mM external Ca^{2+} (supplementary material Fig. S3). The CCE component for each GCaMP2-based sensor was subtracted from the IM data to isolate the effects of non-specific Ca^{2+} entry alone. Cells expressing global GCaMP2, PM-GCaMP2 or GCaMP2-AC2 displayed good sensitivity to IM-induced Ca^{2+} release from non-mobilizable stores and to the subsequent non-specific Ca^{2+} entry seen after the addition of external Ca^{2+} (Fig. 5C). By contrast, GCaMP2-AC8 detected just a small rise in Ca^{2+} during intracellular store release and was unable to detect any significant non-specific Ca^{2+} entry after addition of 0.5 mM external Ca^{2+}, suggesting that the sensor resides in a cellular microdomain that is 'shielded' from ionophore-mediated Ca^{2+} fluxes.

Discussion

In this study, we have investigated whether common Ca^{2+} signalling events such as Ins(1,4,5)P_3-mediated store release or CCE produce different subcellular Ca^{2+} signals. We speculated that Ca^{2+} compartments centred on specific AC isoforms might help to explain the selective responsiveness of Ca^{2+}-sensitive ACs to CCE over other types of Ca^{2+} increase that have been observed in a number of cell types (Burnay et al., 1998; Debernardi et al., 1993; Fagan et al., 2000a; Fagan et al., 1998; Shuttleworth and Thompson, 1999; Watson et al., 1998; Yoshimura and Cooper, 1992). It has been hypothesized that this property might, at least, partially, reflect the residence of these ACs in lipid-raft regions of the PM alongside sites of CCE (Fagan et al., 2000b; Smith et al., 2002). The possibility of functional coupling between the Ca^{2+}-sensitive ACs and known molecular components of CCE channels (STIM1 and Orai) has recently been demonstrated and suggests a degree of intimacy, although direct protein-protein interactions were not detected (Martin et al., 2009). Thus, endogenously expressed Ca^{2+}-sensitive ACs are potentially subjected to large local Ca^{2+} changes during physiological stimuli that trigger store depletion and subsequent refilling of the ER. By contrast, Ca^{2+}-insensitive AC isoforms target to non-raft PM regions (Cooper and Crossthwaite, 2006) and might experience different physiological Ca^{2+} fluxes. Thus, the rationale for the present study was to discern whether the ACs localize in discrete 'Ca^{2+} microdomains' that exhibit diverse Ca^{2+} signals in response to a range of stimuli. By comparing the Ca^{2+} signals seen within the immediate vicinity of the Ca^{2+}-stimulated AC8 and the Ca^{2+}-insensitive AC2 with more widespread Ca^{2+} changes monitored within the bulk cell cytosol or sub-plasmalemmal regions, we would be able to directly establish whether the selectivity of AC8 for CCE is dictated by its residence in a unique Ca^{2+} microdomain.

The Ca^{2+}-inhibitable ACs (AC5 and AC6) display the same functional selectivity for CCE over Ca^{2+} release (Chiono et al., 1995; Fagan et al., 1998; Fagan et al., 2000b). Earlier attempts to directly address the functional disparity of the sensitivity of the Ca^{2+}-inhibitable AC6 to CCE but not to Ca^{2+} release from the ER employed an AC6/aequorin chimera (Nakahashi et al., 1997). When attached to the C-terminus of AC6 and expressed in HEK293 cells, the Ca^{2+}-sensitive photoprotein aequorin reported larger [Ca^{2+}] changes in response to CCE than during Ca^{2+} mobilization, when compared with a cytosolically expressed aequorin. Although this aequorin-based approach gave us the first hints into Ca^{2+} dynamics within the immediate vicinity of a Ca^{2+}-sensitive AC compared with global Ca^{2+} changes, the absolute levels of Ca^{2+} detected by the AC6/aequorin sensor during release and entry were actually remarkably similar, 1160±136 nM and 1225±117 nM, respectively (Nakahashi et al., 1997), and could not explain the selectivity of AC6 for CCE over Ca^{2+} mobilization. A number of limitations, including poor spatial resolution (with a necessity to average signals from cell populations) and difficulties in calibrating the sensor, curtailed further studies based on aequorin. Additionally, attempts to generate an AC8/aequorin chimera were thwarted by mistargeting of AC8 to the cell cytosol and loss of aequorin activity, depending on whether the photoprotein was tagged at the N- or C-terminus of AC8 (our unpublished results). The generation of a GCaMP2-tagged version of AC8 in the present study did not suffer the same technical problems because not only are the activities of the AC and the GCaMP2 unchanged, but the GCaMP2-AC8 is also targeted appropriately to the PM. This has permitted the first single-cell, high resolution Ca^{2+} measurements within the immediate environment of a Ca^{2+}-sensitive AC. By comparing the Ca^{2+} signals reported in HEK293 cells expressing GCaMP2-AC8 and GCaMP2-AC2, we can offer direct evidence that AC8 typically localizes to a subdomain of the PM, where it is exposed to rapid Ca^{2+} fluxes originating from CCE but detects little or no Ca^{2+} change in response to other modes of Ca^{2+} rise. In a subpopulation of GCaMP2-AC8-expressing cells, a response to both Ca^{2+} release and CCE was seen (Fig. 3D), consistent with single-cell cAMP measurements in HEK-AC8 cells in which a subpopulation of the cells responded to both release and entry (Fig. 2D). These data might reflect differences in the targeting or expression levels of AC8 in the two cell populations. The preferred responsiveness of AC8 to CCE is consistent with the sensitivity of AC8 seen in pancreatic cells endogenously expressing this AC isoform (Watson et al., 2001; Martin et al., 2009). However, Ins(1,4,5)P_3-mediated Ca^{2+} release can also stimulate endogenously expressed AC8, as recently demonstrated in pituitary-derived GH_3B_6 cells (Wachten et al., 2010). This suggests that even in its native environment AC8 has the potential to be differentially targeted and/or regulated within the cell. The GCaMP2-AC2 data presented here reveal that the Ca^{2+}-insensitive AC2 resides some distance from sites of CCE and is

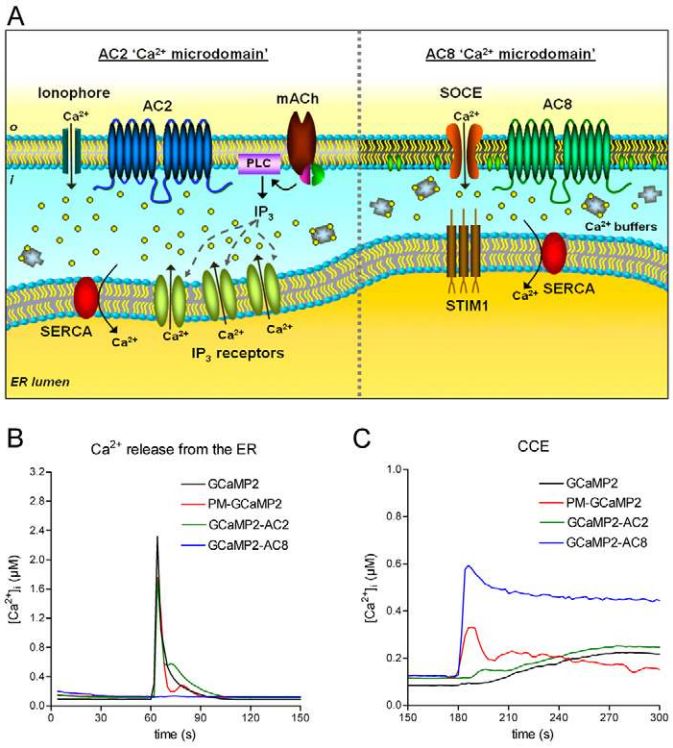

Fig. 6. AC2- and AC8-associated 'Ca^{2+} microdomains' are selective for specific modes of Ca^{2+} rise. (**A**) Cartoon illustrating the possible colocalization of AC2 and AC8 with specific sites of Ca^{2+} entry and release. mACh, muscarinic acetylcholine; SOCE, store-operated Ca^{2+} entry; PLC, phospholipase C; IP_3, inositol-(1,4,5)-trisphosphate (**B**) Calibrated Ca^{2+} signals from single cells expressing each of the four GCaMP2 sensors in response to CCh-induced Ca^{2+} mobilization. (**C**) Calibration of GCaMP2 sensor signals in the same cells during CCE.

subjected to large Ca^{2+} fluxes as a consequence of Ins(1,4,5)P_3-mediated store release or ionophore-mediated Ca^{2+} entry across the PM. The less-selective Ca^{2+} changes detected with GCaMP2-AC2 were comparable to those seen with the global sensor. These findings point towards the targeting of AC8 and AC2 to distinct microdomains of the PM where they appear to colocalize with a different assortment of Ca^{2+} regulatory proteins (Fig. 6A).

We exploited the kinetic properties of the Ca^{2+} chelators EGTA and BAPTA to further test our hypothesis that AC8 resides close to CCE channels. Previously, EGTA and BAPTA have been used as exogenous mobile buffers to model diffusion profiles for Ca^{2+} from its point source within discrete microdomains (Naraghi & Neher, 1995). Elegant studies of the store-operated Ca^{2+} current I_{CRAC} in T lymphocytes utilized the differential abilities of EGTA and BAPTA to perturb Ca^{2+} diffusion during Ca^{2+} entry, and estimated a [Ca^{2+}] of ~1 μM in regions 5-20 nm from the mouth of the channel in the absence of exogenous mobile buffer, with [Ca^{2+}] rising steeply at distances of <5 nm (Zweifach and Lewis, 1995). This value was unchanged in the presence of the relatively slow chelator EGTA, but substitution with the fast chelator BAPTA, dramatically steepened the Ca^{2+} gradient at 5-20 nm from the site of Ca^{2+} entry (Zweifach and Lewis, 1995). Such values, based on single-channel estimates, might be further influenced by neighbouring CRAC channels or saturatable levels of endogenous mobile buffer, which might substantially enhance the spatial distribution of store-mediated Ca^{2+} signals (Parekh, 2008). Our comparison of the effects of the chelators on the GCaMP2 sensor signals revealed that the initial detection of CCE by GCaMP2-AC8 was not perturbed by EGTA [estimated to reach millimolar intracellular concentrations (Tsien, 1981; Tsien et al., 1982)], supporting the hypothesis that AC8 resides very close to sites of CCE. However, the transient nature of the GCaMP2-AC8 signal response to CCE in the presence of EGTA was a little surprising and suggestive of a local acid shifts as a consequence of proton release from EGTA as it chelates cytosolic Ca^{2+} (Tsien, 1980), which could dampen the GCaMP2-AC8 signal [the pKa of GCaMP2 is 7.5 or 6.7 in the absence or presence of Ca^{2+}, respectively (Wang et al., 2008)]. The inability of EGTA to significantly attenuate the peak response of GCaMP2-AC8 to CCE is consistent with previous functional assays in C6-2B glioma cells, which showed that BAPTA loading prevented CCE-mediated inhibition of AC6, whereas EGTA was ineffective (Fagan et al., 1998). Interestingly, the modest Ca^{2+} rises in response to Ins(1,4,5)P_3-mediated Ca^{2+} release seen in a subpopulation of GCaMP2-AC8-expressing cells (Fig. 3D, cell 2) was eliminated in the presence of EGTA (Fig. 4D), suggesting that the source of this Ca^{2+} increase arose more distally with respect to AC8 and was likely to be more readily buffered before it could influence AC8 activity. The ability of PM-GCaMP2 to detect entry of Ca^{2+} via CCE channels was also sensitive to EGTA, which suggested that although the PM-targeted sensor could detect quite rapid increases in the local Ca^{2+} signal (Fig. 3G), the sensor was further from sites of CCE than was GCaMP2-AC8. Although AC8 is targeted to lipid-rich regions of the PM, it is not known whether AC8 preferentially resides in a population of lipid rafts that include proteins such as the plasma membrane Ca^{2+}-ATPase (PMCA) (Sepulveda et al., 2006; Jiang et al., 2007), which could provide a protective microenvironment shielding the AC from non-CCE modes of Ca^{2+} rise. This possibility could explain the higher selectivity of GCaMP2-AC8 for CCE over the PM-GCaMP2 sensor, which might establish more transient associations with lipid rafts due to its simple palmitoylation motif (Resh, 2006).

To estimate the [Ca^{2+}] that are likely to be seen by AC8 and AC2 during Ca^{2+} mobilization and subsequent Ca^{2+} entry in HEK293 cells, the K_d, F_{max} and F_{min} values from GCaMP2 sensor calibrations (supplementary material Fig. S1) were used to estimate typical single-cell responses to CCh-evoked Ca^{2+} release and CCE (Fig. 6B,C, respectively). Large Ca^{2+} rises, in excess of 1 μM, were seen during Ins(1,4,5)P_3-mediated Ca^{2+} release with the global, PM-targeted and AC2-targeted GCaMP2, whereas GCaMP2-AC8 detected no change in local [Ca^{2+}] in the majority of cells tested (Fig. 6B). However, the sensors displayed an inverse discriminatory behaviour with respect to their CCE sensitivity: GCaMP2-AC8 detected the largest rise in Ca^{2+}, which peaked within the first few seconds of stimulating CCE (from a slightly elevated baseline) (Fig. 6C). The peak rise in Ca^{2+} signal detected by GCaMP2-AC8 (593 nM) fell close to the EC_{50} value for in vitro Ca^{2+} stimulation of AC8 activity in HEK293 cell membranes [EC_{50}=560 nM (Masada et al., 2009)]. This value is somewhat smaller than might be predicted for a sensor residing very close to sites of CCE, where local Ca^{2+} signals are estimated to reach ~1 μM (Zweifach and Lewis, 1995). However, we are averaging the GCaMP2-AC8 signal from the entire cell and it is possible that not all of the sensor is directly adjacent to sites of Ca^{2+} entry and/or a proportion of the sensor might be saturating, thereby diluting any estimate of [Ca^{2+}] detected. The influence of endogenous Ca^{2+} buffering (including

the presence of CaM-binding proteins such as AC8 itself, or a close association of AC8 with other proteins such as the PMCA) cannot be excluded, which might further limit the Ca^{2+} signal detected by GCaMP2-AC8. The smaller CCE-mediated Ca^{2+} signal detected by PM-GCaMP2 (332 nM) accords with the sensor being located more distally from CCE sites than AC8, and it might be reasonable to suggest that this sensor only detects Ca^{2+} entering the cell as a consequence of simultaneous CCE through several channels [for instance at STIM1/Orai puncta (Park et al., 2009)]. The response of the global and AC2-targeted sensors was minimal during the first 30 seconds of CCE but increased slowly thereafter as Ca^{2+} gradually diffused from its site of entry into the rest of the cell.

The present study provides direct evidence of an intimate association between AC8 and CCE channels, with other modes of Ca^{2+} increase having little impact on local Ca^{2+} levels within the vicinity of AC8. What remain to be resolved are the mechanisms by which this exclusive Ca^{2+} microdomain is established and maintained. The precise role of lipid-raft targeting is yet to be determined. Clearly, lipid-raft disruption ablates regulation of AC8 by CCE (Fagan et al., 2000b; Smith et al., 2002). However, our perspective of a rigid or stable association between ACs and CCE components in lipid rafts (Fagan et al., 2000b; Smith et al., 2002) is evolving to envisage more dynamic, potentially transient encounters between elements with complementary lipid-binding properties (Martin et al., 2009; Pagano et al., 2009). Nevertheless, the remarkable absence of Ca^{2+} change within the vicinity of AC8 during ionophore-mediated Ca^{2+} entry reported here (Fig. 5C), along with previous evidence of the insensitivity of AC8 to IM-induced Ca^{2+} rises (Fagan et al., 1996), is consistent with heterogeneities within the PM that are characteristic of lipid rafts. Earlier findings that cholesterol enrichment can impede ionophore-mediated Ca^{2+} fluxes in model membranes (Blau and Weissmann, 1988) can be taken to suggest that ionophores insert into non-raft regions of the PM so that the Ca^{2+} movement that they facilitate might be remote from raft-localized ACs. It is conceivable that the lack of response to ionophore mediated Ca^{2+} entry is further enabled by targeting of AC8 to a subdomain of lipid rafts with restricted Ca^{2+} diffusion from the bulk cell cytosol or neighbouring regions of the PM. Physical barriers such as tight associations between the PM and ER (plasmerosomes) (Lee et al., 2006; Mao et al., 2008) or the cytoskeleton (our unpublished results) might contribute to such a distinct AC8-associated Ca^{2+} microdomain. Both mobile and non-diffusible endogenous Ca^{2+} buffers or local Ca^{2+} pumps might also play a key role in restricting the diffusion of Ca^{2+} between neighbouring subcellular compartments. It is even conceivable that adenylyl cyclases and the proteins of the CCE apparatus are intimately associated in a complex, although traditional biochemical methods have found no evidence of such complexes (Martin et al., 2009). However, the different AC-associated Ca^{2+} microdomains that we have identified are potentially amenable to further dissection using the sensors to provide real-time reporting of the domains. More broadly, the direct demonstration of individual AC isoforms residing in distinct Ca^{2+} microdomains shows a tightly regulated system whereby the interplay between dynamic signalling events can take place with maximal efficiency. The evolution of such elegant devices points towards the critical constraints that are placed on these interactions and underlines their physiological importance. It is not unlikely that such dynamic and spatially restricted Ca^{2+} signalling events will prove to be exploited in the regulation and function of other raft-localized proteins.

Materials and Methods

Reagents

Ionomycin and Fura-2-AM were purchased from Merck Chemicals (Nottingham, UK). EGTA-AM, BAPTA-AM, CellMask Deep Red plasma membrane stain and Lipofectamine 2000 were from Invitrogen (Paisley, UK). Restriction enzymes, DNA T4 ligase and calf intestinal phosphatase (CIP) were from New England Biolabs (Ipswich, MA). Oligonucleotides were from Sigma-Genosys (Haverhill, UK). All other reagents were obtained from Sigma-Aldrich (Dorset, UK).

Cell culture and transfection

HEK293 cells (European Collection of Cell Cultures, Porton Down, UK) were grown in minimal essential medium (MEM) supplemented with 10% (v/v) foetal bovine serum, 100 U/ml penicillin, 100 μg/ml streptomycin, 100 μg/ml neomycin and 2 mM L-glutamine and maintained at 37°C in a humidified atmosphere of 95% air and 5% CO_2. One day prior to transient transfection with the construct of choice, the cells were plated onto either 100-mm dishes or 25-mm poly-L-lysine-coated coverslips. The Lipofectamine 2000 method of transfection was used following the manufacturer's instructions and using 2 or 1 μg total cDNA for each 100-mm dish or 25-mm coverslip, respectively. Cells were used ~48 hours post-transfection.

Construction of global GCaMP2, PM-GCaMP2, GCaMP2-AC2 and GCaMP2-AC8

For global GCaMP2, a DNA fragment encoding GCaMP2 was generated by PCR using the pN1-RSET-mG1.6#X-1 plasmid (Nakai et al., 2001) as template. Primer sequences were: forward, 5′-CCGAAGCTTCCACCATGCGGGGTTCTC-3′; and reverse, 5′-CGCTCTAGAACCACCACCCTTCGCTGTCATCATTTGTAC-3′. The reverse primer adds 5′-ACCACCACC-3′ to the codon before last of GCaMP2 (underlined), which encodes three glycines that form part of the sequence linking GCaMP2 to the AC in the fusion constructs GCaMP2-AC2 and GCaMP2-AC8 (see below). The global GCaMP2 DNA-fragment was cloned via *Hind*III(5′)/*Xba*I(3′) into pcDNA3.1zeo (Invitrogen, Paisley, UK) to obtain pcD3.1-globalGCaMP2. To construct PM-GCaMP2, a DNA fragment encoding PM-GCaMP2 was generated by PCR using pcD3.1-GCaMP2 as template. Primer sequences were: forward, 5′-CGAAGCTTCCACCATGGGATGTATCAATAGCAAGCGCAAAGATGCTAG-CATGCGGGTTCTATCATC-3′; and reverse, 5′-CGCTCTAGAACCACCACC-CTTCGCTGTCATCATTTGTAC-3′. The forward primer introduces 5′-ATGGGAT-GTATCAATAGCAAGCGCAAAG-3′ in front of the original ATG of global GCaMP2 (underlined). This leads to the N-terminal modification of global GCaMP2 with the 'SH4' motif (GCINSKRKD) of Lyn kinase. The PM-GCaMP2 DNA-fragment was cloned via *Hind*III(5′)/*Xba*I(3′) into pcDNA3.1zeo (pcD3.1-pmGCaMP2). For GCaMP2-AC2, a DNA fragment encoding full-length AC2 (rat) was generated by PCR using pcD3-AC2 (Feinstein et al., 1991) as template. Primer sequences were: forward, 5′-GCTCTAGAGGGGGGGGGCGGCGGCGCCGCTACC-3′; and reverse, 5′-GCTCTAGATCAGGATGCCAA GTTGCTCTG-3′. The forward primer adds 5′-GGGGGGGGG-3′ before the first codon of *AC2* (underlined); this sequence encodes three glycines that form part of the sequence linking GCaMP2 to AC2 in the fusion construct GCaMP2-AC2. The AC2 DNA-fragment was cloned via *Xba*I(5′ and 3′) into the *Xba*I-cut pcD3.1-globalGCaMP2 (pcD3.1-GCaMP2AC2). Within the fusion protein, GCaMP2 and AC2 are linked via the amino acids GGGSRGGG. To construct GCaMP2-AC8, a DNA fragment encoding full-length AC8 (rat) was generated by PCR using pcD3-AC8 (Cali et al., 1994) as template. Primer sequences were: forward, 5′-CTGTCTAGAGGAGGCGGGGAACTCTCGGATGTGCAC-3′; and reverse, 5′-GCGCTCGAGTTATGGCAAATCGGATTTGTC-3′. The forward primer adds 5′-GGAGGCGGG-3′ before the first codon of *AC8* (underlined); this sequence encodes three glycines that form part of the sequence linking GCaMP2 to AC8 in the fusion construct GCaMP2-AC8. The AC8 DNA-fragment was cut from *Xba*I(5′)/*Xho*I(3′). In a three-fragment ligation, AC8 (*Xba*I/*Xho*I) and global GCaMP2 (*Hind*III/*Xba*I) were cloned into *Hind*III/*Xho*I-cut pcD3.1zeo (pcD3.1-GCaMP2AC8). Within the fusion protein, GCaMP2 and AC8 are linked via GGGSRGGG.

Confocal imaging

Live cell confocal images were obtained using an inverted Zeiss LSM 510 confocal microscope (40× oil objective; NA 1.3). GCaMP2 sensors were excited at 488 nm and emission collected using a 505-550 band pass filter. Parallel images of the CellMask Deep Red PM stain were obtained using excitation at 633 nm and emission collected at >650 nm. Image overlays to determine colocalization were generated using Metamorph imaging software (Molecular Devices).

Cell population measurement of cAMP accumulation

Accumulation of cAMP in intact cells was measured according to the method of Evans et al. (Evans et al., 1984) as described previously (Garritsen and Cooper, 1992) with some modifications. At 2 days post-transfection, HEK293 cells were incubated in MEM (90 minutes at 37°C) with 2-^{3}H-adenine (1.5 μCi per well) to label the ATP pool. The cells were then washed once and incubated with a nominally Ca^{2+}-free Krebs buffer containing 120 mM NaCl, 4.75 mM KCl, 1.44 mM $MgSO_4$, 11 mM glucose, 25 mM HEPES and 0.1% BSA adjusted to pH 7.4 with 2 M Tris base. All experiments were carried out at 30°C in the presence of the phosphodiesterase inhibitor 3-isobutyl-1-methylxanthine (100 μM), which was pre-incubated with the cells for 10 minutes prior to either a 1-minute (AC8) or 15-minute (AC2) assay. To measure

AC8 activity, cells were pre-incubated for 4 minutes with 100 nM Tg in the presence of 100 μM EGTA to prime the cells for CCE. Accumulation of cAMP was measured over a 1-minute period beginning with the addition of 10 μM forskolin (FSK) along with various concentrations of Ca^{2+}. To measure AC2 activity, a 15-minute assay was started by the addition of 100 nM FSK with or without phorbol myristate acetate (PMA, 100 nM) or phorbol dibutyrate (PDBu, 100 nM), in the presence of 1 mM Ca^{2+}. Assays were terminated by the addition of ice-cold 5% (w/v final concentration) trichloroacetic acid. ^{3}H-cAMP was formed from ^{3}H-ATP and quantified as previously described (Evans et al., 1984; Garritsen and Cooper, 1992). Results are presented as the means ± s.d. of triplicate determinations.

Epac2-camps FRET measurements

Fluorescent imaging of Epac2-camps-expressing HEK293 cells was performed using an Andor Ixon+ EMCCD camera (Andor, Belfast, UK) and an Optosplit (505DC) to separate CFP (470 nm) and YFP (535 nm) emission images (Cairn Research, Kent, UK). For dual-emission ratio imaging, cells were excited at 435 nm using a monochromator (Cairn Research) and 51017 filter set (Chroma) attached to a Nikon eclipse TE2000-S microscope (40× objective). Emission images at 470 nm and 535 nm were collected every 3-5 seconds (250-millisecond integration time) and analysed using Metamorph imaging software (Molecular Devices). Cells in which the CFP and YFP fluorescence intensity was less than twice the background signal were excluded, as were cells with excessive expression of the fluorescent probe. Single-cell FRET data were plotted as changes in background-subtracted 470 nm versus 535 nm (CFP/YFP) emission ratio.

Fura-2 Ca^{2+} measurements

Cells were plated onto 25 mm poly-L-lysine-coated coverslips 24 hours prior to loading with 4 μM Fura-2/AM and 0.02% Pluronic F-127 (Molecular Probes, Leiden) for 40 minutes at room temperature in extracellular buffer containing 140 mM NaCl, 4 mM KCl, 1 mM $CaCl_2$, 0.2 mM $MgCl_2$, 11 mM D-glucose, 10 mM HEPES, pH 7.4. After loading, cells were washed several times and imaged using a CoolSNAP-HQ CCD camera (Photometrics) and monochromator system (Cairn Research, Kent, UK) attached to a Nikon TMD microscope (40× objective). Emission images (D510/80M) at 340 nm and 380 nm excitation were collected at 1 Hz using MetaFluor software (Molecular Devices). For zero calcium buffer, 1 mM $CaCl_2$ was omitted and replaced by 100 μM EGTA.

GCaMP2 measurements

Ca^{2+} measurements using GCaMP2-based constructs were performed using an Ixon+ EMCCD camera (Andor). Cells were excited at 488 nm using a monochromator (Cairn Research) and ET-GFP filter set (with 495DC and 525/50 emitter) (Chroma) attached to a Nikon eclipse TE2000-S microscope (40× objective). Emission images were collected every 3-5 seconds (250-300 millisecond integration time), background-subtracted, and analysed using Metamorph imaging software (Molecular Devices). For in situ calibration of the GCaMP2 constructs, cells were washed with zero calcium buffer and then the external solution was switched to an 'intracellular-like saline' (ICS) containing 140 mM KCl, 4 mM NaCl, 1.4 mM $MgCl_2$, 10 mM HEPES, 1 mM EGTA, plus 50 μg/ml of saponin, pH 7.4 (using KOH). After 5-10 minutes in the permeabilizing ICS solution, cells were exposed to a number of standard calibration solutions containing ICS plus increasing concentrations of free Ca^{2+} (ranging from 0 up to ~8 μM, as estimated using the programme WinmaxC (available at www.stanford.edu/~cpatton/maxc.html). The solution was changed every 30 seconds giving rise to a stepped increase in emission signal. As expected, treatment with saponin resulted in some diffusion of the global sensor from the cell. Fluorescence was plotted as a function of the maximum and minimum GCaMP2 signal obtained $[\log (F\text{-}F_{min})/(F_{max}\text{-}F)]$ versus $\log [Ca^{2+}]$ to determine the K_d and Hill coefficient for each GCaMP2 sensor (supplementary material Fig. S1A). The fit of the calibration data (obtained using Prism) becomes less linear at concentrations above 800 nM, leading to some potential error (overestimate) of the peak calibrated $[Ca^{2+}]$ reached during Ins(1,4,5)P_3-induced release. The impact of F_{max} and K_d values on the calibration curves was also examined (see supplementary material Fig. S1B,C) and showed a clear relationship between F_{max} and the calibration range of the GCaMP2 sensors.

Many thanks to Michael Kotlikoff (Cornell University, New York, NY) and Martin Lohse (Würzberg University, Germany) for the kind gifts of plasmid DNA encoding GCaMP2 and Epac2-camps, respectively. This work was funded by The Wellcome Trust (RG 31760). DMFC is a Royal Society Wolfson Research Fellow. Deposited in PMC for release after 6 months.

Supplementary material available online at
http://jcs.biologists.org/cgi/content/full/123/1/107/DC1

References

Abrams, T. W., Karl, K. A. and Kandel, E. R. (1991). Biochemical studies of stimulus convergence during classical conditioning in Aplysia: dual regulation of adenylate cyclase by Ca^{2+}/calmodulin and transmitter. *J. Neurosci.* **11**, 2655-2665.

Alicia, S., Angelica, Z., Carlos, S., Alfonso, S. and Vaca, L. (2008). STIM1 converts TRPC1 from a receptor-operated to a store-operated channel: moving TRPC1 in and out of lipid rafts. *Cell Calcium* **44**, 479-491.

Blau, L. and Weissmann, G. (1988). Transmembrane calcium movements mediated by ionomycin and phosphatidate in liposomes with Fura 2 entrapped. *Biochemistry* **27**, 5661-5666.

Burnay, M. M., Vallotton, M. B., Capponi, A. M. and Rossier, M. F. (1998). Angiotensin II potentiates adrenocorticotrophic hormone-induced cAMP formation in bovine adrenal glomerulosa cells through a capacitative calcium influx. *Biochem. J.* **330**, 21-27.

Cali, J. J., Zwaagstra, J. C., Mons, N., Cooper, D. M. F. and Krupinski, J. (1994). Type VIII adenylyl cyclase. A Ca^{2+}/calmodulin-stimulated enzyme expressed in discrete regions of rat brain. *J. Biol. Chem.* **269**, 12190-12195.

Chiono, M., Mahey, R., Tate, G. and Cooper, D. M. F. (1995). Capacitative Ca^{2+} entry exclusively inhibits cAMP synthesis in C6-2B glioma cells. Evidence that physiologically evoked Ca^{2+} entry regulates Ca^{2+}-inhibitable adenylyl cyclase in non-excitable cells. *J. Biol. Chem.* **270**, 1149-1155.

Cooper, D. M. F. and Crossthwaite, A. J. (2006). Higher-order organization and regulation of adenylyl cyclases. *Trends Pharmacol. Sci.* **27**, 426-431.

Cooper, D. M. F., Mons, N. and Karpen, J. W. (1995). Adenylyl cyclases and the interaction between calcium and cAMP signalling. *Nature* **374**, 421-424.

Debernardi, M. A., Munshi, R. and Brooker, G. (1993). Ca^{2+} inhibition of beta-adrenergic receptor- and forskolin-stimulated cAMP accumulation in C6-2B rat glioma cells is independent of protein kinase C. *Mol. Pharmacol.* **43**, 451-458.

Dyachok, O., Isakov, Y., Sagetorp, J. and Tengholm, A. (2006). Oscillations of cyclic AMP in hormone-stimulated insulin-secreting beta-cells. *Nature* **439**, 349-352.

Evans, T., Smith, M. M., Tanner, L. I. and Harden, T. K. (1984). Muscarinic cholinergic receptors of two cell lines that regulate cyclic AMP metabolism by different molecular mechanisms. *Mol. Pharmacol.* **26**, 395-404.

Fagan, K. A., Mahey, R. and Cooper, D. M. F. (1996). Functional co-localization of transfected Ca^{2+}-stimulable adenylyl cyclases with capacitative Ca^{2+} entry sites. *J. Biol. Chem.* **271**, 12438-12444.

Fagan, K. A., Mons, N. and Cooper, D. M. F. (1998). Dependence of the Ca^{2+}-inhibitable adenylyl cyclase of C6-2B glioma cells on capacitative Ca^{2+} entry. *J. Biol. Chem.* **273**, 9297-9305.

Fagan, K. A., Graf, R. A., Tolman, S., Schaack, J. and Cooper, D. M. F. (2000a). Regulation of a Ca^{2+}-sensitive adenylyl cyclase in an excitable cell. Role of voltage-gated versus capacitative Ca^{2+} entry. *J. Biol. Chem.* **275**, 40187-40194.

Fagan, K. A., Smith, K. E. and Cooper, D. M. F. (2000b). Regulation of the Ca^{2+}-inhibitable adenylyl cyclase type VI by capacitative Ca^{2+} entry requires localization in cholesterol-rich domains. *J. Biol. Chem.* **275**, 26530-26537.

Feinstein, P. G., Schrader, K. A., Bakalyar, H. A., Tang, W. J., Krupinski, J., Gilman, A. G. and Reed, R. R. (1991). Molecular cloning and characterization of a Ca^{2+}/calmodulin-insensitive adenylyl cyclase from rat brain. *Proc. Natl. Acad. Sci. USA* **88**, 10173-10177.

Ferguson, G. D. and Storm, D. R. (2004). Why calcium-stimulated adenylyl cyclases? *Physiology (Bethesda)*. **19**, 271-276.

Garritsen, A. and Cooper, D. M. F. (1992). Manipulation of intracellular calcium in NCB-20 cells. *J. Neurochem.* **59**, 190-199.

Gu, C. and Cooper, D. M. F. (2000). Ca^{2+}, Sr^{2+}, and Ba^{2+} identify distinct regulatory sites on adenylyl cyclase (AC) types VI and VIII and consolidate the apposition of capacitative cation entry channels and Ca^{2+}-sensitive ACs. *J. Biol. Chem.* **275**, 6980-6986.

Guillou, J.-L., Nakata, H. and Cooper, D. M. F. (1999). Inhibition by calcium of mammalian adenylyl cyclases. *J. Biol. Chem.* **274**, 35539-35545.

Isshiki, M., Ying, Y. S., Fujita, T. and Anderson, R. G. (2002). A molecular sensor detects signal transduction from caveolae in living cells. *J. Biol. Chem.* **277**, 43389-43398.

Jacobowitz, O., Chen, J., Premont, R. T. and Iyengar, R. (1993). Stimulation of specific types of Gs-stimulated adenylyl cyclases by phorbol ester treatment. *J. Biol. Chem.* **268**, 3829-3832.

Jiang, L., Fernandes, D., Mehta, N., Bean, J. L., Michaelis, M. L. and Zaidi, A. (2007). Partitioning of the plasma membrane Ca^{2+}-ATPase into lipid rafts in primary neurons: effects of cholesterol depletion. *J. Neurochem.* **102**, 378-388.

Landa, L. R., Harbeck, M., Kaihara, K., Chepurny, O., Kitiphongspattana, K., Graf, O., Nikolaev, V. O., Lohse, M. J., Holz, G. G. and Roe, M. W. (2005). Interplay of Ca^{2+} and cAMP signaling in the insulin-secreting MIN6 beta-cell line. *J. Biol. Chem.* **280**, 31294-31302.

Lee, M. Y., Song, H., Nakai, J., Ohkura, M., Kotlikoff, M. I., Kinsey, S. P., Golovina, V. A. and Blaustein, M. P. (2006). Local sub-plasmamembrane Ca^{2+} signals detected by a tethered Ca^{2+} sensor. *Proc. Natl. Acad. Sci. USA* **103**, 13232-13237.

Mao, T., O'Connor, D. H., Scheuss, V., Nakai, J. and Svoboda, K. (2008). Characterization and subcellular targeting of GCaMP-type genetically-encoded calcium indicators. *PLoS ONE* **3**, e1796.

Marsault, R., Murgia, M., Pozzan, T. and Rizzuto, R. (1997). Domains of high Ca^{2+} beneath the plasma membrane of living A7r5 cells. *EMBO J.* **16**, 1575-1581.

Martin, A. C. and Cooper, D. M. F. (2006). Capacitative and 1-oleyl-2-acetyl-sn-glycerol-activated Ca^{2+} entry distinguished using adenylyl cyclase type 8. *Mol. Pharmacol.* **70**, 769-777.

Martin, A. C., Willoughby, D., Ciruela, A., Ayling, L.-J., Pagano, M., Wachten, S., Tengholm, A. and Cooper, D. M. F. (2009). Capacitative Ca^{2+} entry via Orai1 and stromal interacting molecule 1 (STIM1) regulates adenylyl cyclase type 8. *Mol. Pharmacol.* **75**, 830-842.

Masada, N., Ciruela, A., Macdougall, D. A. and Cooper, D. M. F. (2009). Distinct mechanisms of regulation by Ca^{2+}/calmodulin of type 1 and 8 adenylyl cyclases support their different physiological roles. *J. Biol. Chem.* **284**, 4451-4463.

McDougall, D. A., Wachten, S., Ciruela, A., Sinz, A. and Cooper, D. M. F. (2009). Separate elements within a single IQ-like motif in adenylyl cyclase type 8 impart Ca^{2+}/calmodulin binding and autoinhibition. *J. Biol. Chem.* **284**, 15573-15588.

Nakahashi, Y., Nelson, E., Fagan, K. A., Gonzales, E., Guillou, J. L. and Cooper, D. M. F. (1997). Construction of a full-length Ca^{2+}-sensitive adenylyl cyclase/aequorin chimera. *J. Biol. Chem.* **272**, 18093-18097.

Nakai, J., Ohkura, M. and Imoto, K. (2001). A high signal-to-noise Ca^{2+} probe composed of a single green fluorescent protein. *Nat. Biotechnol.* **19**, 137-141.

Naraghi, M. and Neher, E. (1997). Linearized buffered Ca^{2+} diffusion in microdomains and its implications for calculation of [Ca^{2+}] at the month of a calcium channel. *J. Neurosci.* **17**, 6961-6973.

Nicol, X., Bennis, M., Ishikawa, Y., Chan, G. C. K., Reperant, J., Storm, D. R. and Gaspar, P. (2006). Role of the calcium modulated cyclases in the development of the retinal projections. *Eur. J. Neurosci.* **24**, 3401-3414.

Nikolaev, V. O., Bunemann, M., Hein, L., Hannawacker, A. and Lohse, M. J. (2004). Novel single chain cAMP sensors for receptor-induced signal propagation. *J. Biol. Chem.* **279**, 37215-37218.

Pagano, M., Clynes, M. A., Masada, N., Ciruela, A., Ayling, L.-J., Wachten, S. and Cooper, D. M. F. (2009). Insights into the residence in lipid rafts of adenylyl cyclase AC8 and its regulation by capacitative calcium entry. *Am. J. Phys.* **296,** C607-C619.

Pani, B., Ong, H. L., Liu, X., Rauser, K., Ambudkar, I. S. and Singh, B. B. (2008). Lipid rafts determine clustering of STIM1 in endoplasmic reticulum-plasma membrane junctions and regulation of store-operated Ca^{2+} entry (SOCE). *J. Biol. Chem.* **283**, 17333-17340.

Parekh, A. B. (2008). Ca^{2+} microdomains near plasma membrane Ca^{2+} channels: impact on cell function. *J. Physiol.* **586**, 3043-3054.

Park, C. Y., Hoover, P. J., Mullins, F. M., Bachhawat, P., Covington, E. D., Raunser, S., Walz, T., Garcia, K. C., Dolmetsch, R. E. and Lewis, R. S. (2009). STIM1 clusters and activates CRAC channels via direct binding of a cytosolic domain to Orai1. *Cell* **136**, 876-890.

Rapp, P. E. and Berridge, M. J. (1977). Oscillations in calcium-cyclic AMP control loops form the basis of pacemaker activity and other high frequency biological rhythms. *J. Theor. Biol.* **66**, 497-525.

Rasmussen, H. and Goodman, D. B. (1977). Relationships between calcium and cyclic nucleotides in cell activation. *Physiol. Rev.* **57**, 421-509.

Resh, M. D. (2006). Palmitoylation of ligands, receptors, and intracellular signaling molecules. *Sci. STKE*. **359**, re14.

Sepulveda, M. R., Berrocal-Carrillo, M., Gasset, M. and Mata, A. M. (2006). The plasma membrane Ca^{2+}-ATPase isoform 4 is localized in lipid rafts of cerebellum synaptic plasma membranes. *J. Biol. Chem*. **281**, 447-453.

Shuttleworth, T. J. and Thompson, J. L. (1999). Discriminating between capacitative and arachidonate-activated Ca^{2+} entry pathways in HEK293 cells. *J. Biol. Chem.* **274**, 31174-31178.

Smith, K. E., Gu, C., Fagan, K. A., Hu, B. and Cooper, D. M. F. (2002). Residence of adenylyl cyclase type 8 in caveolae is necessary but not sufficient for regulation by capacitative Ca^{2+} entry. *J. Biol. Chem*. **277**, 6025-6031.

Tallini, Y. N., Ohkura, M., Choi, B. R., Ji, G., Imoto, K., Doran, R., Lee, J., Plan, P., Wilson, J., Xin, H. B. et al. (2006). Imaging cellular signals in the heart in vivo: Cardiac expression of the high-signal Ca^{2+} indicator GCaMP2. *Proc. Natl. Acad. Sci. USA* **103**, 4753-4758.

Tsien, R. Y. (1980). New calcium indicators and buffers with high selectivity against magnesium and protons: Design, synthesis, and properties of prototype structures. *Biochemistry* **19**, 2396-2404.

Tsien, R. Y. (1981). A non-disruptive technique for loading calcium buffers and indicators into cells. *Nature* **290**, 527-528.

Tsien, R. Y., Pozzan, T. and Rink, T. J. (1982). Calcium homeostasis in intact lymphocytes: cytoplasmic free calcium monitored with a new, intracellularly trapped fluorescent indicator. *J. Cell Biol.* **94**, 325-334.

Wachten, S., Masada, N., Ayling, L.-J., Ciruela, A., Nikolaev, V. O., Lohse, M. J. and Cooper, D. M. F. (2010). Distinct pools of cAMP centre on different isoforms of adenylyl cyclase in pituitary-derived GH_3B_6 cells. *J. Cell Sci.* **123**, 95-106.

Wang, Q., Shui, B., Kotlikoff, M. I. and Sondermann, H. (2008). Structural basis for calcium sensing by GCaMP2. *Structure* **16**, 1817-1827.

Watson, E. L., Wu, Z., Jacobson, K. L., Storm, D. R., Singh, J. C. and Ott, S. M. (1998). Capacitative Ca^{2+} entry is involved in cAMP synthesis in mouse parotid acini. *Am. J. Physiol.* **274**, C557-C565.

Willoughby, D. and Cooper, D. M. F. (2006). Ca^{2+} stimulation of adenylyl cyclase generates dynamic oscillations in cyclic AMP. *J. Cell Sci.* **119**, 828-836.

Willoughby, D. and Cooper, D. M. F. (2007). Organization and Ca^{2+} regulation of adenylyl cyclases in cAMP microdomains. *Physiol. Rev.* **87**, 965-1010.

Wu, Z., Wong, S. T. and Storm, D. R. (1993). Modification of the calcium and calmodulin sensitivity of the type I adenylyl cyclase by mutagenesis of its calmodulin binding domain. *J. Biol. Chem.* **268**, 23766-23768.

Yoshimura, M. and Cooper, D. M. F. (1992). Cloning and expression of a Ca^{2+}-inhibitable adenylyl cyclase from NCB-20 cells. *Proc. Natl. Acad. Sci. USA* **89**, 6716-6720.

Yoshimura, M. and Cooper, D. M. F. (1993). Type-specific stimulation of adenylyl cyclase by protein kinase C. *J. Biol. Chem.* **268**, 4604-4607.

Zweifach, A. and Lewis, R. S. (1995). Rapid inactivation of depletion-activated calcium current (I_{CRAC}) due to local calcium feedback. *J. Gen. Physiol.* **105**, 209-226.

Journal of Cell Science